Biomaterials Science

ROYAL SOCIETY OF CHEMISTRY

PAPER

View Article Online
View Journal

Cite this: DOI: 10.1039/d0bm01823f

Interventional nuclear medicine: "click" chemistry as an *in vivo* targeting strategy for imaging microspheres and bacteria†

M. M. Welling, [a] N. Duszenko, [a,b] D. M. van Willigen,[a] A. W. Hensbergen, [a] T. Buckle, [a] D. D. D. Rietbergen, [a,c] M. Roestenberg [b] and F. W. B. van Leeuwen *[a]

Aim: Pre-targeting is a proven strategy for *in vivo* delivery of a diagnostic or therapeutic payload. The pre-targeting concept can be realized through various conjugation strategies, one of which is based on copper-free "click" chemistry. Copper-free click reactions have shown *in vivo* potential for imaging and radionuclide therapy, but this conjugation strategy has not yet been explored in combination with microspheres or unicellular organisms. This study aims to evaluate the *in vivo* efficacy of strain-promoted azide–alkyne cycloaddition (SPAAC) reactions to achieve imaging and targeting of azide-functionalized macro-aggregated albumin (MAA) microspheres and *Staphylococcus aureus* bacteria. *Methods*: MAA microspheres (diameter 10–90 μm) were functionalized with a biorthogonal Cy5 fluorophore, bearing an azide functionality (N_3), to generate MAA-Cy5-N_3. *S. aureus* (diameter ~1 μm) were functionalized with ^{99m}Tc-UBI$_{29-41}$-Cy5-N_3, generating *S. aureus*-^{99m}Tc-UBI$_{29-41}$-Cy5-N_3. *In situ* and *in vitro* click conjugation on the $-N_3$ moieties was studied for 20 h using a radioactivity-based assay and fluorescence microscopy. For *in vivo* validation, both primary entities, radiolabeled with ^{99m}Tc, were deposited into the microvasculature of the liver *via* intrasplenic injections. Secondary targeting was realized following the intravenous administration of indium-111-radiolabeled diethylenetriaminepentaacetic acid-dibenzocyclooctyne (^{111}In-DTPA-DBCO). To assess click reaction efficiency *in vivo*, ^{99m}Tc and ^{111}In-biodistributions were measured (SPECT and %ID g^{-1}). Use of ^{111}In-DTPA-DBCO in mice without MAA deposits or mice infected with non-functionalized *S. aureus* served as controls. *Ex vivo* confocal fluorescence imaging was carried out in excised tissues to confirm the presence of functionalized MAA and bacteria. *Results: In vitro* data confirmed effective click reactions on both the MAA particles and the bacterial membrane. SPECT imaging and biodistribution studies revealed significantly ($p < 0.05$) increased accumulation of ^{111}In-DTPA-DBCO at the sites where MAA-Cy5-N_3 (7.5 ± 1.5% ID g^{-1} *vs.* 3.5 ± 0.5%ID g^{-1} in control mice) and *S. aureus*-^{99m}Tc-UBI$_{29-41}$-Cy5-N_3 (9.3 ± 1.3%ID g^{-1} *vs.* 6.0 ± 0.5%ID g^{-1} in control mice) resided. *Ex vivo* fluorescence imaging confirmed the presence of either functionalized MAA or *S. aureus* in excised spleens and livers of mice. *Conclusion*: Copper-free click chemistry between a DBCO moiety and Cy5-N_3-functionalized microspheres or bacterial entities in the liver can be used to realize *in vivo* imaging and targeting.

Received 26th October 2020,
Accepted 22nd December 2020

DOI: 10.1039/d0bm01823f

rsc.li/biomaterials-science

Introduction

Precision medicine, broadly defined as interventions that factor in patients' unique characteristics, is rapidly emerging as the standard of care in many disciplines.[1,2] In this respect, interventional nuclear medicine provides a good example. Within the discipline, nuclear medicine based imaging can be used to direct the delivery of therapy. Guided by disease-specific antigens, this process has the intention to induce more specific treatment, better outcomes, and fewer unwanted side effects.[3,4] The guidance approach has recently been expanded with pre-targeting strategies. Recently, tumor-specific antigens have been labeled with a reactive moiety that then enables a secondary vector to home in on the target *via* the specific marker. Such strategies can help ameliorate undesirable characteristics of certain compounds, such as high background activity in imaging or substantial toxicity to non-

[a]*Interventional Molecular Imaging Laboratory, Department of Radiology, Leiden University Medical Center, Albinusdreef 2, 2300 RC, Leiden, Netherlands. E-mail: f.w.b.van_leeuwen@lumc.nl*
[b]*Departments of Parasitology and Infectious Diseases, Leiden University Medical Center, Leiden, Netherlands*
[c]*Section of Nuclear Medicine, Department of Radiology, Leiden University Medical Center, Leiden, Netherlands*

†Electronic supplementary information (ESI) available. See DOI: 10.1039/d0bm01823f

target tissue in treatment.[5–7] The targeting concept also allows the use of secondary agents carrying radionuclides with lower effective dose values and concomitantly lesser side effects.[6,8–11]

Specific chemical interactions *in vivo* can be achieved using reactive moieties not natively found in biological systems. One such interaction that has gained traction over the past decade is click chemistry. The most widely used reaction, the strain-promoted azide–alkyne cycloaddition (SPAAC), makes use of biorthogonal ligands (*e.g.*, azide ($-N_3$) with DBCO) not found in biological systems.[12–14] As a chemical ligand for functionalization, $-N_3$ is particularly suitable due to several properties: it is small, inert towards substrates in the cellular environment, and possesses favorable modes of reactivity.[15] SPAAC has been successfully employed *in vitro*,[16] in drug targeting,[17,18] pre-targeted radioimmunotherapy,[19] drug depositing approaches,[20] and cell-tracking studies.[21,22]

Recently, we have shown the value of the pre-targeting concept in a liver radioembolization model using supramolecular chemistry.[23,24] Here, reduced hemodynamics in the liver vasculature enabled the host–guest complexation of a targeting vector onto adamantane functionalized macro-aggregated albumin (MAA) microspheres. We hypothesized that SPAAC reaction may also benefit from the reduced hemodynamics and could be applied in a liver embolization model for either MAA-N_3 or *S. aureus*-$UBI_{29–41}$-Cy5-N_3. To address this hypothesis, we targeted these pre-functionalized and transplanted entities with ^{111}In-labeled diethylenetriaminepentaacetic acid-dibenzocyclooctyne (^{111}In-DTPA-DBCO) in an *in vivo* vascular embolization model in the liver.

Materials and methods

Synthesis

General. All chemicals were obtained from commercial sources and were used without further purification. Solvents were dried using molecular sieves unless stated otherwise. The reactions were monitored by thin-layer chromatography (TLC) and/or mass spectrometry using a Bruker microflex™ LRF MALDI-TOF. Column chromatography was performed using SiliaFlash Irregular Silica Gel, P60, 40–63 μm, 60 Å (Screening Devices BV, Amersfoort, The Netherlands). HPLC was performed on a Waters (Etten-Leur, The Netherlands) HPLC system using a 1525EF or 2545 pump and a 2489 UV/VIS detector. For preparative HPLC either a Waters XBridge Prep C8 10 μm OBD (30 × 250 mm) column (25 mL min^{-1}) or a Dr Maisch GmbH (Ammerbuch, Germany) Reprosil-Pur 120 C18-AQ 10 μm (250 × 20 mm) column (12 mL min^{-1}) were used. For semi-preparative HPLC a Dr Maisch GmbH Reprosil-Pur C18-AQ 10 μm (250 × 10 mm) column was used (5 mL min^{-1}). For analytical HPLC a Dr Maisch GmbH Reprosil-Pur C18-AQ 5 μm (250 × 4.6 mm) column was used applying a gradient of 0.1% TFA in H_2O/CH_3CN 95 : 5 to 0.1% TFA in H_2O/CH_3CN 5 : 95 in 40 min (1 mL min^{-1}). NMR spectra were recorded using a Bruker DPX-300 spectrometer (300 MHz ^{1}H NMR, 75 MHz ^{13}C NMR) and chemical shifts (δ) are reported relative to TMS (δ = 0) and/or referenced to the solvent in which they were measured.

Radio-HPLC was performed on a Jasco HPLC system using an MD-2010 UV-Vis absorption detector, PU-2080 pumps, DG-2080-53 degasser, MX-2080-31 solvent mixer, LC-Net II/ADC interface (Jasco Benelux B.V., De Meern, The Netherlands) connected with an on-line Raytest Gabi radioactivity-HPLC-flow monitor, 1 × 1″ well-type NaI scintillation detector (Elysia Raytest Benelux, Angleur, Belgium). For analysis, a Hi-Load C18 5 μm Type 202TP54 column (250 × 4.6 mm), (GraceVydac, Grace Corporate, CO) was used. 10 μL samples were injected and a gradient of 0.1% TFA in H_2O/CH_3CN 95 : 5 to 0.1% TFA in H_2O/CH_3CN 5 : 95 in 50 min (1 mL min^{-1}) was applied.

Cy5-N_3 Pfp ester. Cy5-N_3 was synthesized as previously described.[25] For the Pfp ester, Cy5-N_3 (10 mg. 12.5 μmol), bis (pentafluorophenyl) carbonate (10 mg, 25 μmol) and NMM (6 μL, 50 μmol) were dissolved in DMF (1.5 mL) and the mixture was stirred at room temperature (r.t.). After completion, the solvent was evaporated *in vacuo* and the crude was purified by preparative HPLC. After pooling the fractions containing the product, the solution was lyophilized yielding a blue solid. MALDI-TOF: $[M + 2H]^+$ calcd 878.9; found 878.7. The compound was dissolved in DMSO and the 11.4 mM solution was stored at −21 °C until use.

DTPA-DBCO

DTPA-DBCO was synthesized as previously described.[26] MALDI-TOF: $[M + H]^+$ calcd 722.3; found 723.0. ^{1}H-NMR (300 MHz, D_2O) δ 7.67 (s, 2H), 7.65–7.37 (m, 8H), 5.11–5.06 (d, 2H), 3.96 (s, 8H) 3.86–3.82 (d, 2H), 3.45 (t, 4H), 3.37 (s, 2H), 3.05 (t, 4H), 2.52–2.50 (m, 2H), 2.21 (m, 2H).

See ESI Fig. S1B.†

$UBI_{29–41}$-Cy5-N_3. Synthesis and characterization of $UBI_{29–41}$-Cy5-N_3 (2241.5 Da) were carried out as previously described.[27]

Conjugation of MAA with Cy5-N_3 Pfp ester

Lyophilized macro-aggregated albumin (MAA, clinical grade 2 mg Pulmocis®, Curium, Den Bosch, The Netherlands) was suspended in 1 mL of saline (0.9% NaCl, sterile and pyrogen-free, B. Braun Medical Supplies, Inc., Oss, The Netherlands) and aliquots of 0.1 mL were stored at −21 °C until use. To one portion of MAA (0.1 mL, 2 mg mL^{-1}) 5 μL Cy5-N_3 Pfp ester (50 μg, 57 nmol) was added and the mixture was shaken overnight at 37 °C. PBS was added and the blue reaction mixture was centrifuged (5 min at 1500*g*) and decanted. This was repeated until the supernatant remained colorless. The remaining blue pellet consisting of MAA-Cy5-N_3 was resuspended in 0.1 mL PBS. Additionally, confocal microscopy was performed to visually confirm the staining of MAA with Cy5-N_3. Of the solution containing MAA-Cy5-N_3, 10 μL was pipetted onto culture dishes with glass inserts (Ø35 mm glass-bottom dishes no. 15, poly-D-lysine coated, γ-irradiated, MatTek corporation). Images were acquired in a single field of view using a Leica SP5 WLL confocal microscope (λ_{ex} 633 nm, λ_{em} 650–700 nm) under 100× magnification using Leica Application Suite software.

Radiolabeling

Preparation of ^{99m}Tc-MAA-Cy5-N_3. To facilitate imaging and co-localization of the pre-targeted MAA with the ^{111}In labeled DBCO tracer *in vivo* before the preparation of MAA-Cy5-N_3 as described above. MAA was first labeled with ^{99m}Tc. To one aliquot of MAA, 0.1 mL of a freshly eluted $^{99m}TcO_4^-$ solution (500 MBq mL^{-1}, Mallinckrodt Medical B.V.) was added and the suspension was gently shaken in a water bath for 1 h at 37 °C. To remove free $^{99m}TcO_4^-$, PBS was added followed by centrifugation (5 min at 1500*g*), which was repeated. The degree of labeling in the pellet containing ^{99m}Tc-MAA-Cy5-N_3 was calculated using the following formula:

$$\text{Radiochemical yield}\,(\%) = \frac{\text{radioactivity}_{\text{pellet}}}{\text{radioactivity}_{\text{pellet}} + \text{radioactivity}_{\text{supernatant}}} \cdot 100.$$

To the resulting suspension, 5 μL of Cy5-N_3 Pfp ester in DMSO (11.4 mM) was added and the solution was shaken for 1 h at 37 °C. Unconjugated fluorophore was removed by the addition of PBS and centrifuged twice at 1500*g* for 5 min. After decanting, the pellet was resuspended in 1 mL PBS and was directly used for the experiments.

Labeling of UBI$_{29-41}$-Cy5-N_3 with ^{99m}Tc was carried out as previously described.[27]

^{111}In-DTPA-DBCO. DTPA-DBCO was labeled with ^{111}In according to a previously published method.[28] Briefly, 52.8 μL of DTPA-DBCO in 250 mM NH_4OAc pH 5.5 (200 μL) was added to 25–150 μL of an acidic solution of $^{111}InCl_3$ (370 MBq mL^{-1}, Mallinckrodt Medical, Petten, The Netherlands). After gently shaking for 60 min at r.t., 700 μL of PBS was added to the reaction mixture and the solution was used as-is. A schematic structure and the ^{1}H-NMR of ^{111}In-DTPA-DBCO are shown in Fig. S1A and B.† The radiochemical purity was determined by thin-layer chromatography (TLC) using H_2O as mobile phase as well as by radio-HPLC. The elution of radioactivity corresponded with that of DTPA-DBCO was calculated using the following formula:

$$\text{Radiochemical yield}\,(\%) = \frac{\text{radioactivity}_{\text{DTPA-DBCO}}}{\text{radioactivity}_{\text{DTPA-DBCO}} + \text{radioactivity}_{\text{unbound}}} \cdot 100.$$

The calculations revealed a 95% labeling yield of ^{111}In-DTPA-DBCO (Fig. S2†). DTPA-DBCO (3.8 mg, 5.3 μmol) was dissolved in 0.1 M HEPES buffer pH 7.4 where after $^{111}InCl_3$ (52.6 μL of a 200 mM solution, 1051 μmol) was added and the mixture was shaken at r.t. After 3 h, H_2O 0.1% TFA and CH_3CN 0.1% TFA were added and the mixture was purified by HPLC. After combining the product containing fractions and lyophilization, a pink solid was obtained. MALDI-TOF calcd 834.55, found 834.98. As additional steps of characterization, lipophilicity (log *P*), and serum protein interactions of ^{111}In-DTPA-DBCO were determined. The log *P* was measured using the conventional shake-flask method involving octanol and water and the serum binding (PPB) was measured using RED plates (Merck, St Louis, USA), both methods performed according to Hensbergen *et al.*[26] The lipophilicity partition coefficient log $P_{(o/w)}$ was found to be −1.09 ± 0.02 (n = 6). An increase in lipophilicity leads to higher binding to plasma proteins which affects the liver and bowel retention.[28,29] The plasma protein binding yielded a serum binding of 95.0 ± 2.0% (n = 6).

Preparation of *S. aureus*-^{99m}Tc-UBI$_{29-41}$-Cy5-N_3. Labeling of *Staphylococcus aureus* (*S. aureus* ATCC 29213, Manassas, VA 20108 USA) with ^{99m}Tc-UBI$_{29-41}$-Cy5-N_3 was carried out as described before,[27] except with a 10-fold higher amount of peptide to increase peptide loading of bacteria, allowing intensified click reactions *in vivo*. For labeling, a stock vial containing 3 × 10^9 viable *S. aureus* per mL was defrosted, washed three times (4 min × 3500 rpm) in 25 mM Na–NH_4–acetate (pH 5). Next, 100 μL of ^{99m}Tc-UBI$_{29-41}$-Cy5-N_3 (1.5 μM in 25 mM Na–NH_4–acetate, pH 5; 100 MBq) was added to 1 mL of the bacterial suspension containing 2 × 10^8 viable *S. aureus*, and the mixture was gently stirred at r.t. To determine the load of bacterial membranes with ^{99m}Tc-UBI$_{29-41}$-Cy5-N_3 the radioactivity in relation to bacteria was quantitated after 2 times washing steps with PBS and by 2 centrifugation steps (5 min at 3500*g*). The yield of labeling in the bacterial pellet containing ^{99m}Tc-UBI$_{29-41}$-Cy5-N_3 was calculated using the method as for the labeling of ^{99m}Tc-MAA-Cy5-N_3.

Assessment of staining and viability of *S. aureus*-^{99m}Tc-UBI$_{29-41}$-Cy5-N_3. Additionally, confocal microscopy and analysis were performed to visually confirm the staining of *S. aureus* with Hoechst and UBI$_{29-41}$-Cy5-N_3 as described before.[27] Specifically, 4.3 × 10^6 *S. aureus* in 10 μL were added to a glass-bottom microwell dish (MatTek Corporation, Ashland, MA, USA) and overlaid with a coverslip, following which images were acquired on a Leica Sp8 WLL confocal microscope using LAS X software.

Viability of labeled bacteria, compared to unlabeled bacteria, was assessed by serially diluting equivalent quantities of bacteria, plating 10 μL aliquots of each dilution onto BHI agar plates, incubating overnight at 37 °C, and finally counting CFUs the following day.

In vitro click and stability experiments

To test the efficacy of the bioorthogonal click reactions *in vitro*, mixtures of 0.1 mL saline containing either 0.1 mg MAA-Cy5-N_3 or 1 × 10^8 labelled *S. aureus*-UBI$_{29-41}$-Cy5-N_3 with 0.1 mL (10 μg mL^{-1}, 1 MBq) of ^{111}In-DTPA-DBCO were diluted with 0.8 mL PBS and the suspensions were incubated for 1 h in a shaking water bath at 37 °C (Fig. 1A). After 2 repeats of centrifugation (5 min at 1500*g*), decanting and resuspension to remove non-reacted entities, both complexes were resuspended in FCS and incubated for 1 h in a shaking water bath at 37 °C. Samples were taken at 1 h, 4 h, and 20 h and after 2 washing steps and centrifugation, the reaction efficiency was determined to measure the radioactivity present in the pellet and supernatant in a dose-calibrator. After correction for decay and radioactivity in PBS controls without either MAA or *S. aureus*, the amount of binding to the pellet overtime was expressed as the percentage of the total amount of radioactivity (% binding).

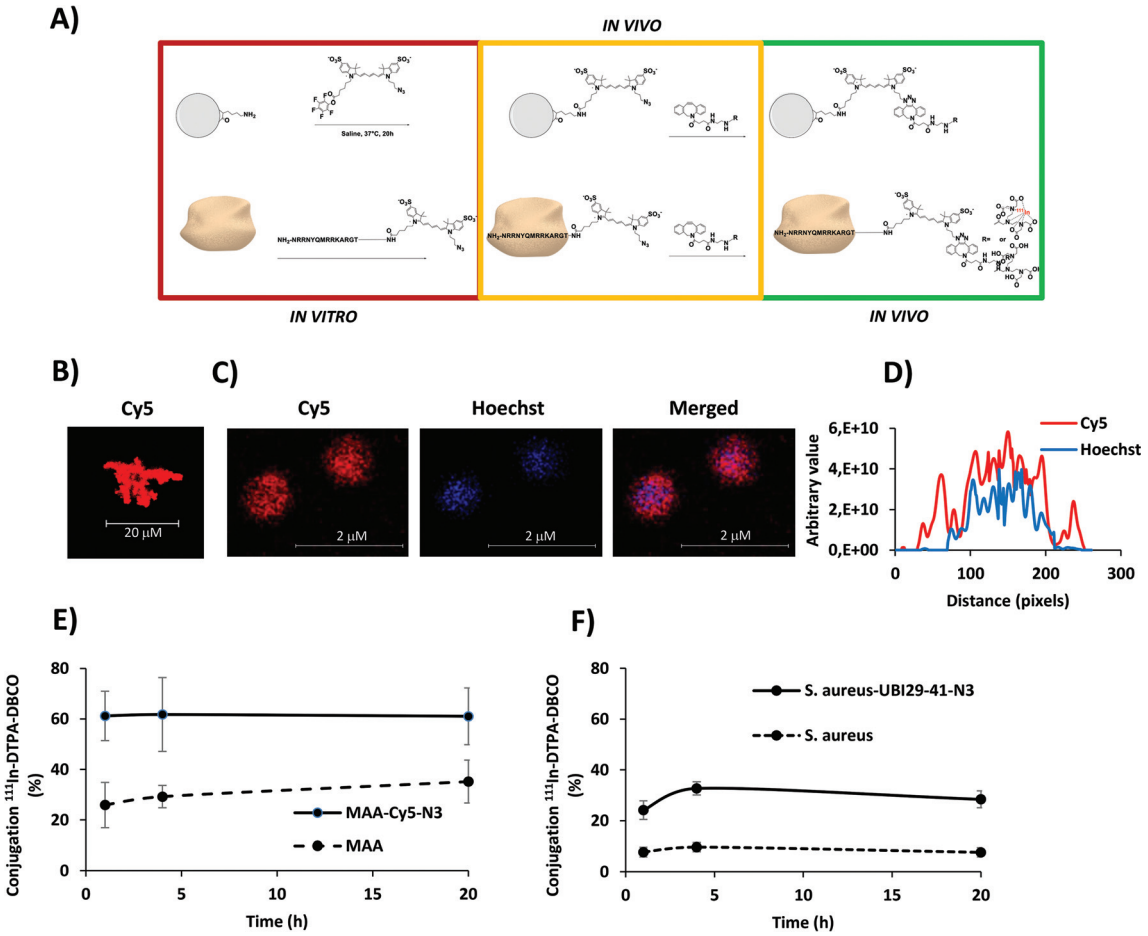

Fig. 1 (A) Schematic presentation of the click reaction between ^{99m}Tc-MAA-Cy5-N_3 or *S. aureus*-^{99m}Tc-UBI$_{29-41}$-Cy5-N_3 and ^{111}In-DTPA-DBCO, which is in agreement with previous reports.[27,31] (B) Fluorescent microscopic imaging of a single MAA-Cy5-N_3 particle (red) and (C) *S. aureus*-UBI$_{29-41}$-Cy5-N_3 demonstrates a high signal of Cy5 fluorescent signal on the membrane and inside the cell at 1000× magnification. (D) Analysis of a plotted section of a single bacterium with two plot profiles. (E) Time-dependent click reaction between ^{99m}Tc-MAA-Cy5-N_3 or unlabeled MAA and ^{111}In-DTPA-DBCO. Data are expressed as the percentage (%) conjugation of MAA and radiolabeled DBCO derivative at various intervals until 20 h of incubation (n = 4). (F) Time-dependent click reaction between *S. aureus*-^{99m}Tc-UBI$_{29-41}$-Cy5-N_3 or unlabeled *S. aureus* and ^{111}In-DTPA-DBCO. Data are expressed as the percentage (%) conjugation between *S. aureus* and radiolabeled DBCO derivative at various intervals until 20 h of incubation (n = 6).

Imaging and biodistribution experiments

Animal model. *In vivo* studies were performed using 2–4-month-old Swiss mice (20–35 g, Crl : OF1 strain, Charles River Laboratories, USA). All animal experiments were approved by the local ethics committee of the Leiden University Medical Center. The experiments were performed in accordance with the Experiments on Animals Act (Wet op de Dierproeven, 2014), which is the applicable legislation in The Netherlands following the European Union guidelines (EU directive 2010/63/EU) regarding the protection of animals used for scientific purposes. All animal experiments were executed in an establishment of the Leiden University Medical Center licensed for the use and housing of experimental animals. All animal studies were approved by the Institutional Animal Ethics Committee (DEC permit 12160) of the Leiden University Medical Center.

An embolization set-up of the liver with functionalized and radiolabeled ^{99m}Tc-MAA-Cy5-N_3 or 1×10^8 *S. aureus*-^{99m}Tc-UBI$_{29-41}$-Cy5-N_3 *via* intra-splenic administration was performed according to previously described procedures,[23,24] After 2 h, ^{111}In-DTPA-DBCO was intravenously injected and longitudinal dual-isotope SPECT imaging was performed. Dual isotope imaging was performed at (i) 140 keV to determine a load of ^{99m}Tc-labeled pre-targeting particles in the liver after intra-splenic administration and at (ii) 240 keV to image the whole-body biodistribution of ^{111}In-DTPA-DBCO. Imaging of ^{111}In-DTPA-DBCO in mice without hepatic embolization with MAA or mice hepatically infected with 1×10^8 unlabeled *S. aureus* (from the same stock) served as controls.

SPECT and fluorescence imaging and biodistribution studies. SPECT imaging and image generation after injection of ^{111}In-DTPA-DBCO was performed in an energy window range set at 240 keV at 2 h, 4 h, or 20 h on a U-SPECT scanner (MILabs, Utrecht, The Netherlands) as previously described.[23,24] Briefly, for reconstruction, the photo peak energy window was centered at 140 keV (^{99m}Tc) or 240 keV

(^{111}In) with a window width of 20%. Side windows of 5% were applied to correct for scatter and down scatter corrections. The image was reconstructed using 24 Pixel based Ordered Subset Expectation Maximization iterations (POSEM) with 4 subsets, 0.2 mm isotropic voxel size and with decay and triple energy scatter correction integrated into the reconstruction with a post filter setting of 0.25 mm. Images were analyzed using Matlab R2014a software (version 8.3.0.532, MathWorks® Natick, MA). Images were generated from 4 mm slices of maximum intensity protocols (MIP) adjusting the color scale set to optimal depiction of the tissues of interest. Because of the physical decay of the radioisotope at 20 h p.i. these images were adjusted with higher contrast. After imaging the mice were euthanized by an intraperitoneal injection of 0.25 mL Euthasol (ASTfarma, Oudewater, The Netherlands). In hepatically infected mice SPECT images were obtained in mice only at 4 h after infection as in previous studies because we observed infection-related detrimental symptoms at 24 h after hepatical bacteria administration.[27] After the *in vivo* imaging studies animals were sacrificed and various tissues including blood and urine samples were excised and weighed. To confirm the liver accumulation of ^{99m}Tc-MAA-Cy5-N_3 or *S. aureus*-^{99m}Tc-$UBI_{29–41}$-Cy5-N_3 the Cy5 content in the spleen and liver were also imaged *ex vivo* using an IVIS Spectrum fluorescence imaging modality. Hereafter, the radioactive content was quantitatively determined using a gamma counter. Finally, the bacterial load in excised and homogenized livers was determined by plating of serial dilutions as described above.

Statistical analysis

All data are presented as mean value (±SD) of 3–5 independent measurements. Statistical analysis for differences between groups in the animal studies was performed by Student's unpaired *T*-test with the two-tailed distribution. Significance was assigned for *p*-values <0.05. All analyses and calculations were performed using Microsoft® Office Excel 2010 and GraphPad Prism version 5.01 for Windows (GraphPad Software, San Diego, CA, USA).

Results

In vitro click reactions

Confocal fluorescence microscopy confirmed the presence of the Cy5 fluorophore on both MAA (Fig. 1B) and *S. aureus* (Fig. 1C & D). For MAA, fluorescence imaging showed a bright signal and intense uptake throughout the entire particle (Fig. 1B), whereas for *S. aureus* the uptake of $UBI_{29–41}$-Cy5-N_3 was less bright and located on the outer membrane and intracellular. An intracellular $UBI_{29–41}$-Cy5 signal was not observed in earlier studies[27,30] but this can be attributed to the five-fold higher dose of $UBI_{29–41}$-Cy5 compared to earlier studies (Fig. 1D). As a result of the higher dose of $UBI_{29–41}$-Cy5-N_3 the viability of *S. aureus*-^{99m}Tc-$UBI_{29–41}$-Cy5-N_3 was significantly reduced (69%; $p < 0.01$). The *in vitro* co-localization of ^{111}In-DTPA-DBCO and MAA increased two-fold after functionalization of MAA with Cy5-N_3 ($p < 0.01$) (Fig. 1E). This extended to a three-fold increase for interactions between ^{111}In-DTPA-DBCO and *S. aureus*-^{99m}Tc-$UBI_{29–41}$-Cy5-N_3 ($p < 0.001$) (Fig. 1F). The click reaction between ^{111}In-DTPA-DBCO and MAA-Cy5-N_3, however, had a reaction efficiency that was about two-fold higher than for *S. aureus*-^{99m}Tc-$UBI_{29–41}$-Cy5-N_3. Binding of ^{111}In-DTPA-DBCO to non-functionalized MAA, which comprises of albumin, is most likely due to the high serum protein binding (95.0 ± 2.0) induced by DBCO.[26]

In vivo imaging of ^{99m}Tc-MAA-Cy5-N_3 and *S. aureus*-^{99m}Tc-$UBI_{29–41}$-Cy5-N_3

To determine the rate of hepatic pre-targeting both radioactivity (^{99m}Tc) and fluorescence (Cy5) imaging of ^{99m}Tc-MAA-Cy5-N_3 was performed. SPECT imaging of the liver of mice after intra-splenic administration with ^{99m}Tc-MAA-Cy5-N_3 showed splenic (injection site) and hepatic uptake of the compound at all intervals until 20 h p.i. (Fig. 2A & B). The radioactive signal was most prominent at 2 h p.i. and declined in time due to the physical decay of ^{99m}Tc ($t_{1/2}$ = 6 h). The fluorescence signal, which is not subjected to radioactive decay, further confirmed the presence of ^{99m}Tc-MAA-Cy5-N_3 in the liver as illustrated in Fig. S3A & S3B.† At 4 h, SPECT imaging similarly revealed *S. aureus*-^{99m}Tc-$UBI_{29–41}$-Cy5-N_3 accumulation in the spleen and liver, which could be confirmed by *ex vivo* fluorescence imaging (Fig. S3C & S3D†).

In vivo imaging of ("clicked") ^{111}In-DTPA-DBCO

At 20 h p.i dual-isotope imaging revealed uptake of ^{111}In-DTPA-DBCO ($t_{1/2}$ ^{111}In = 2.9 days; 240 keV window) in the liver as with early SPECT images of ^{99m}Tc-MAA-Cy5-N_3 (140 keV window), amounting to 7.5 ± 1.5%ID g^{-1} (Fig. 2C & Table S1†). This uptake was significantly ($p < 0.05$) 2-fold higher than the liver uptake of this compound in mice without hepatic pre-targeting (3.5 ± 0.5%ID g^{-1}). As depicted in Table S1,† liver-blood ratios with hepatic pre-targeting (29.8 ± 6.9) were significantly higher than without (16.8 ± 3.3; $p < 0.05$). Intense signals of deposits of radioactivity were observed in the intestines and urine/bladder at various intervals after injection (Fig. 2A & Table S1†).

Dual isotope imaging also revealed the co-localization of ^{111}In-DTPA-DBCO with *S. aureus*-^{99m}Tc-$UBI_{29–41}$-Cy5-N_3. At this interval, hepatic uptake of ^{111}In-DTPA-DBCO amounted to 9.3 ± 1.3%ID g^{-1} (Fig. 3B & Table S2†) which was significantly ($p < 0.05$) higher than the liver uptake of this compound in mice that received a *S. aureus* inoculation (6.0 ± 0.5%ID g^{-1}).

SPECT imaging for intravenously injected ^{111}In-DTPA-DBCO in the absence of any pre-targeting showed hepatobiliary and renal clearance of the tracer. Also, intense signals of deposits of radioactivity were observed in the gall bladder, intestines, and urine/bladder (80.1 ± 5.9 percentage injected dose; %ID as determined with biodistribution studies) at 2 h p.i. (Fig. 2C & Table S1†).

At the end of the imaging experiment, we determined the number of viable bacteria in excised tissues, and found no sig-

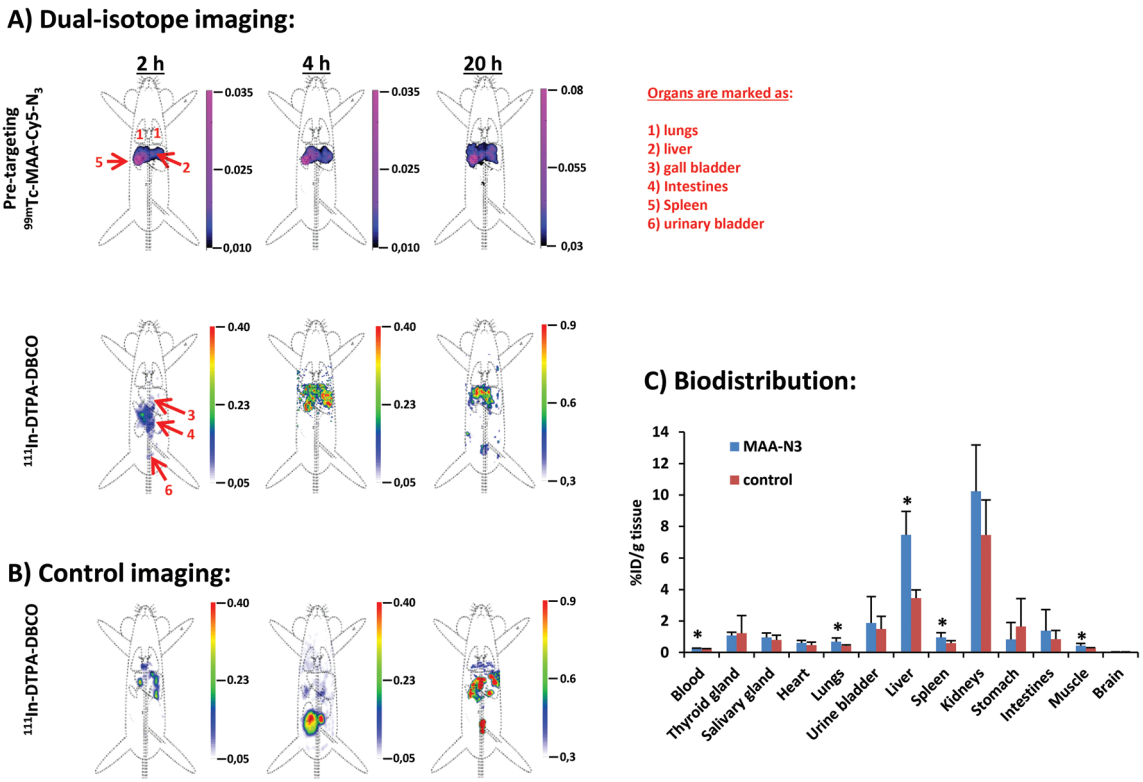

Fig. 2 A&B SPECT data of reconstructed (MIP) scintigraphic 4 mm coronal projections after dual-isotope SPECT imaging of mice injected with MAA. 2 h before SPECT mice were pre-targeted with ^{99m}Tc-MAA-Cy5-N_3 and imaging was performed at various intervals after intravenous administration of ^{111}In-DTPA-DBCO. Dual isotope imaging shows ^{99m}Tc-activity in the spleen and liver (top panel A) and hepatic uptake of ^{111}In-DTPA-DBCO (bottom panel A). (B) SPECT imaging of ^{111}In-DTPA-DBCO only without pre-targeting with bacteria (control). The scale bars represents the intensity of uptake expressed in arbitrary units. (C) Quantified biodistribution of ^{111}In-DTPA-DBCO at 20 h p.i. (%ID g^{-1}) after hepatic pre-targeting with ^{99m}Tc-MAA-Cy5-N_3 (blue bars) or ^{99m}Tc-MAA controls (orange bars). Data (expressed as the mean ± SD of the percentage of the injected dose per gram tissue (%ID g^{-1}) of 3–5 observations. Significance between the models ($p < 0.05$) is indicated with *.

nificant differences in bacterial outgrowth between *S. aureus*-^{99m}Tc-UBI$_{29-41}$-Cy5-N_3 ($1.8 \pm 0.3 \times 10^7$ colony forming units per g liver) and non-labelled *S. aureus* ($2.0 \pm 0.2 \times 10^7$ colony forming units per g liver).

Discussion

In this study, we underscore the feasibility of click chemistry to track the accumulation and/or dissemination of N_3- and ^{99m}Tc-functionalized microspheres and live bacteria *in vivo* using radiolabeled ^{111}In-DTPA-DBCO. Subsequent dual-isotope SPECT imaging visualized the co-localization of both the target and ^{111}In-DTPA-DBCO. Findings were confirmed by biodistribution studies and fluorescence imaging.

In the two liver inoculation models used (^{99m}Tc-MAA-Cy5-N_3 and *S. aureus*-^{99m}Tc-UBI$_{29-41}$-Cy5-N_3), we observed hepatic ^{111}In-DTPA-DBCO uptake at SPECT imaging and in biodistribution measurements (%ID g^{-1}). However, the effectivity of the click reaction varied between models, a phenomenon that was also observed during *in vitro* click assays. The efficacy of click reactions is known to be dependent on the coordination of azide-linked moieties,[15,32–34] a feature that may well vary between Cy5-N_3 Pfp ester and UBI$_{29-41}$-Cy5-N_3. Recently, faster bioorthogonal reactions have become available, such as with the inverse-electron-demand-Diels–Alder (IEDDA reaction),[35] which would be worth exploring in future studies, especially when using less lipophilic compounds. Despite the differences in the efficacy of the click reaction in this study *in vitro*, in mice, both N_3-moieties yielded similar uptake of the ^{111}In-DTPA-DBCO vector.[6,34] Due to the lipophilic character of DTPA-DBCO and the resulting interaction with albumin proteins and bacterial membranes we noticed non-specific binding of ^{111}In-DTPA-DBCO to non-functionalized MAA and *S. aureus*. Nevertheless, functionalization of micro-particles with N_3 yielded 1.6–2.2 times higher binding than non-functionalized MAA and bacteria, and the contribution of this functionalization step herein was always significant.

The ^{111}In-DTPA-DBCO targeting moiety used in this study represents a flexible tracer with respect to these considerations: its small size and relatively low lipophilicity ($\log P_{(o/w)} = -1.09 \pm 0.02$) resulted in rapid renal clearance.[28] Rapid clearance of tracers, as we observed with ^{111}In-DTPA-DBCO, can be beneficial, as it yields high target-to-blood ratios that generally result in lesser toxicity or radiation burdening in non-targeted tissues when such compounds carry therapeutic drugs or radioisotopes, as in radioembolization settings for microspheres.[6,36] To date, no toxic side effects have been

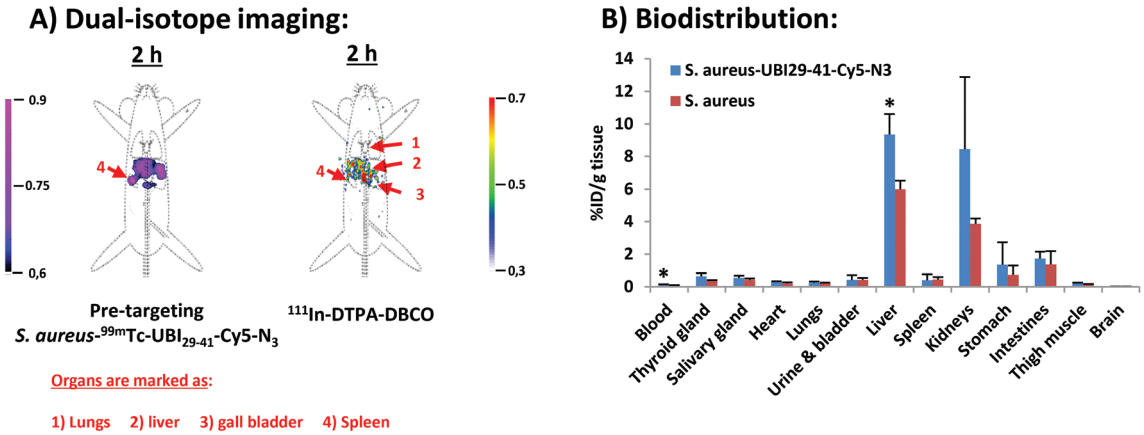

Fig. 3 SPECT data of reconstructed (MIP) scintigraphic 4 mm coronal projections after dual-isotope SPECT imaging of mice. (A) 2 h before SPECT mice were pre-targeted with *S. aureus*-^{99m}Tc-UBI$_{29-41}$-Cy5-N$_3$ and imaging was performed 2 h after intravenous administration of ^{111}In-DTPA-DBCO. Dual isotope imaging shows ^{99m}Tc-activity in the spleen and liver (right panel) and hepatic uptake of ^{111}In-DTPA-DBCO (left panel). The scale bars represents the intensity of uptake expressed in arbitrary units. (B) Quantified biodistribution of ^{111}In-DTPA-DBCO at 2 h p.i. (%ID g^{-1}) after hepatic pre-targeting with *S. aureus*-^{99m}Tc-UBI$_{29-41}$-Cy5-N$_3$ (blue bars) or unlabeled *S. aureus* controls (orange bars). Data (expressed as the mean ± SD of the percentage of the injected dose per gram tissue (%ID g^{-1}) of 3–5 observations. Significance between the models ($p < 0.05$) is indicated with *.

reported for this compound,[37–40] with the only real drawback being that for smaller molecules the incorporation of the DBCO moiety may change the biodistribution of a tracer (*e.g.* when an increase in serum binding alters hepatic uptake).[26] A way to reduce serum protein binding, is to increase their hydrophilicity using, for example, PEG linkers.[41]

In diagnostics and therapy, precise imaging of pathogens can provide valuable information regarding the intensity of infectious burden and monitoring the effect of antimicrobial therapy.[42] Although the clinical application is still several steps away and particularly dependent on the specificity of the pre-targeting azide-bearing moiety, one immediately attractive application of this study's pre-targeting setup is as a platform for monitoring (non-GMO) bacterial colonization and persistence, which could lead to a better understanding of the interactions of pathogens with the immune parameters involved.[30] As UBI$_{29-41}$-peptides have proven their potential to target bacterial infections *in vivo* (including in humans),[43–45] one may even postulate that ^{99m}Tc-UBI$_{29-41}$-Cy5-N$_3$ may in the future be used to target bacterial colonies following intravenous administration. This concept would be in line with previous results that we obtained using ^{111}In-DTPA-UBI$_{29-41}$-Cy5.[46]

Additional studies with implant-related, aged, or chronic infection models are needed to further substantiate the translational impact of the click chemistry presented in this report. Here it should, however, be noted that infections with biofilms could limit uptake of the tracer.

Conclusion

In conclusion, we have here shown that chemistry can be used to target DBCO-linked moieties to N$_3$ pre-targeted entities in mice, which can form the basis for a platform for tracking the fate and dissemination of microspheres and living cells *in vivo*.

Conflicts of interest

The authors have declared that no competing interest exists.

Acknowledgements

We acknowledge Matthias N. van Oosterom and Sven I. van Leeuwen for their assistance with the graphics. The research leading to these results was funded with grants from the Netherlands Organization for Scientific Research (NWO-TTW-VICI grant (TTW 16141).

References

1 D. A. Chambers, W. G. Feero and M. J. Khoury, *J. Am. Med. Assoc.*, 2016, **315**, 1941–1942.
2 I. S. Kohane, *Science*, 2015, **349**, 37–38.
3 J. Gardiazabal, M. Esposito, P. Matthies, A. Okur, J. Vogel, S. Kraft, B. Frisch, T. Lasser and N. Navab, in *Medical Image Computing and Computer-Assisted Intervention – MICCAI 2014*, ed. N. Hata, P. Golland, C. Barillot, J. Hornegger and R. Howe, Springer International Publishing, Cham, 2014, pp. 504–511, DOI: 10.1007/978-3-319-10404-1_63.
4 H. R. Kulkarni, A. Singh, T. Langbein, C. Schuchardt, D. Mueller, J. Zhang, C. Lehmann and R. P. Baum, *Br. J. Radiol.*, 2018, **91**, 20180308.
5 T. Lammers, F. Kiessling, W. E. Hennink and G. Storm, *J. Controlled Release*, 2012, **161**, 175–187.

6 E. J. L. Stéen, P. E. Edem, K. Nørregaard, J. T. Jørgensen, V. Shalgunov, A. Kjaer and M. M. Herth, *Biomaterials*, 2018, **179**, 209–245.
7 M. Altai, R. Membreno, B. Cook, V. Tolmachev and B. M. Zeglis, *J. Nucl. Med.*, 2017, **58**, 1553–1559.
8 B. A. Khaw, K. S. Gada, V. Patil, R. Panwar, S. Mandapati, A. Hatefi, S. Majewski and A. Weisenberger, *Eur. J. Nucl. Med. Mol. Imaging*, 2014, **41**, 1603–1616.
9 G. Paganelli, M. Bartolomei, M. Ferrari, M. Cremonesi, G. Broggi, G. Maira, C. Sturiale, C. Grana, G. Prisco and M. Gatti, *Cancer Biother. Radiopharm.*, 2001, **16**, 227–235.
10 F. Dosio, P. Magnani, G. Paganelli, A. Samuel, G. Chiesa and F. Fazio, *J. Nucl. Biol. Med.*, 1993, **37**, 228–232.
11 A. Rondon and F. Degoul, *Bioconjugate Chem.*, 2020, **31**, 159–173.
12 H. Koo, S. Lee, J. H. Na, S. H. Kim, S. K. Hahn, K. Choi, I. C. Kwon, S. Y. Jeong and K. Kim, *Angew. Chem., Int. Ed.*, 2012, **51**, 11836–11840.
13 K. Nwe and M. W. Brechbiel, *Cancer Biother.Radiopharm.*, 2009, **24**, 289–302.
14 M. Boyce and C. R. Bertozzi, *Nat. Methods*, 2011, **8**, 638.
15 E. M. Sletten and C. R. Bertozzi, *Angew. Chem., Int. Ed.*, 2009, **48**, 6974–6998.
16 K. E. Beatty, J. D. Fisk, B. P. Smart, Y. Y. Lu, J. Szychowski, M. J. Hangauer, J. M. Baskin, C. R. Bertozzi and D. A. Tirrell, *ChemBioChem*, 2010, **11**, 2092–2095.
17 J. D. Thomas, H. Cui, P. J. North, T. Hofer, C. Rader and T. R. Burke, Jr., *Bioconjugate Chem.*, 2012, **23**, 2007–2013.
18 X. Cheng, J. Li, K. Tanaka, U. Majumder, A. Z. Milinichik, A. C. Verdi, C. J. Maddage, K. A. Rybinski, S. Fernando, D. Fernando, M. Kuc, K. Furuuchi, F. Fang, T. Uenaka, L. Grasso and E. F. Albone, *Mol. Cancer Ther.*, 2018, **17**, 2665–2675.
19 K. M. Au, A. Tripathy, C. P.-I. Lin, K. Wagner, S. Hong, A. Z. Wang and S. I. Park, *ACS Nano*, 2018, **12**, 1544–1563.
20 M. R. Adams, C. T. Moody, J. L. Sollinger and Y. Brudno, *Mol. Pharmaceutics*, 2020, **17**, 392–403.
21 K. Kusamori, Y. Takayama and M. Nishikawa, *Curr. Protoc. Stem Cell Biol.*, 2018, **47**, e66.
22 J.-K. Yoon, B.-N. Park, W.-Y. Shim, J. Y. Shin, G. Lee and Y. H. Ahn, *Nucl. Med. Biol.*, 2010, **37**, 381–388.
23 S. J. Spa, M. M. Welling, M. N. van Oosterom, D. D. D. Rietbergen, M. C. Burgmans, W. Verboom, J. Huskens, T. Buckle and F. W. B. van Leeuwen, *Theranostics*, 2018, **8**, 2377–2386.
24 M. M. Welling, S. J. Spa, D. M. van Willigen, D. D. D. Rietbergen, M. Roestenberg, T. Buckle and F. W. B. van Leeuwen, *J. Controlled Release*, 2019, **293**, 126–134.
25 S. van der Wal, C. M. de Korne, L. G. L. Sand, D. M. van Willigen, P. C. W. Hogendoorn, K. Szuhai, F. W. B. van Leeuwen and T. Buckle, *ChemBioChem*, 2018, **19**, 1758–1765.
26 A. W. Hensbergen, D. M. van Willigen, M. M. Welling, F. A. van der Wijk, C. M. de Korne, M. N. van Oosterom, M. Schottelius, H.-J. Wester, T. Buckle and F. W. B. van Leeuwen, *ACS Omega*, 2019, **4**, 12438–12448.
27 M. M. Welling, C. M. de Korne, S. J. Spa, D. M. van Willigen, A. W. Hensbergen, A. Bunschoten, N. Duszenko, W. K. Smits, M. Roestenberg and F. W. B. van Leeuwen, *ACS Infect. Dis.*, 2019, **5**, 1160–1168.
28 A. Bunschoten, D. M. van Willigen, T. Buckle, N. S. van den Berg, M. M. Welling, S. J. Spa, H. J. Wester and F. W. B. van Leeuwen, *Bioconjugate Chem.*, 2016, **27**, 1253–1258.
29 A. W. Hensbergen, T. Buckle, D. M. van Willigen, M. Schottelius, M. M. Welling, F. A. van der Wijk, T. Maurer, H. G. van der Poel, G. van der Pluijm, W. M. van Weerden, H.-J. Wester and F. W. B. van Leeuwen, *J. Nucl. Med.*, 2020, **61**, 234–241.
30 N. Duszenko, D. M. van Willigen, M. M. Welling, C. M. de Korne, R. van Schuijlenburg, B. M. F. Winkel, F. W. B. van Leeuwen and M. Roestenberg, *ACS Infect. Dis.*, 2020, **6**, 1734–1744.
31 M. M. Welling, N. Duszenko, D. M. Van Willigen, W. K. Smits, M. Roestenberg, T. Buckle and F. W. B. van Leeuwen, Submitted for publication.
32 L. Carroll, H. L. Evans, E. O. Aboagye and A. C. Spivey, *Org. Biomol. Chem.*, 2013, **11**, 5772–5781.
33 S. V. Orski, G. R. Sheppard, S. Arumugam, R. M. Arnold, V. V. Popik and J. Locklin, *Langmuir*, 2012, **28**, 14693–14702.
34 S. M. M. Dadfar, S. Sekula-Neuner, U. Bog, V. Trouillet and M. Hirtz, *Small*, 2018, **14**, 1800131.
35 S. Mushtaq, S.-J. Yun and J. Jeon, *Molecules*, 2019, **24**, 3567.
36 L. O. Gainkam, V. Caveliers, N. Devoogdt, C. Vanhove, C. Xavier, O. Boerman, S. Muyldermans, A. Bossuyt and T. Lahoutte, *Contrast Media Mol. Imaging*, 2011, **6**, 85–92.
37 P. V. Chang, J. A. Prescher, E. M. Sletten, J. M. Baskin, I. A. Miller, N. J. Agard, A. Lo and C. R. Bertozzi, *Proc. Natl. Acad. Sci. U. S. A.*, 2010, **107**, 1821–1826.
38 R. Rossin, P. R. Verkerk, S. M. van den Bosch, R. C. Vulders, I. Verel, J. Lub and M. S. Robillard, *Angew. Chem., Int. Ed.*, 2010, **49**, 3375–3378.
39 Y. Brudno, R. M. Desai, B. J. Kwee, N. S. Joshi, M. Aizenberg and D. J. Mooney, *ChemMedChem*, 2015, **10**, 617–620.
40 S. M. J. van Duijnhoven, R. Rossin, S. M. van den Bosch, M. P. Wheatcroft, P. J. Hudson and M. S. Robillard, *J. Nucl. Med.*, 20155, **56**, 1422–1428.
41 J. S. Suk, Q. Xu, N. Kim, J. Hanes and L. M. Ensign, *Adv. Drug Delivery Rev.*, 2016, **99**, 28–51.
42 M. M. Welling, A. W. Hensbergen, A. Bunschoten, A. H. Velders, M. Roestenberg and F. W. B. van Leeuwen, *Clin. Transl. Imaging*, 2019, **7**, 105–124.
43 A. Ostovar, M. Assadi, K. Vahdat, I. Nabipour, H. Javadi and M. Eftekhari, *Clin. Nucl. Med.*, 2013, **38**, 413–416.
44 C. A. de Murphy, F. Gemmel and J. Balter, *Nucl. Med. Commun.*, 2010, **31**, 726–733.
45 G. Ferro-Flores, M. A. Avila-Rodríguez and F. O. García-Pérez, *Clin. Transl. Imaging*, 2016, **4**, 175–182.
46 M. M. Welling, A. Bunschoten, J. Kuil, R. Nelissen, F. J. Beekman, T. Buckle and F. W. B. van Leeuwen, *Bioconjugate Chem.*, 2015, **26**, 839–849.

